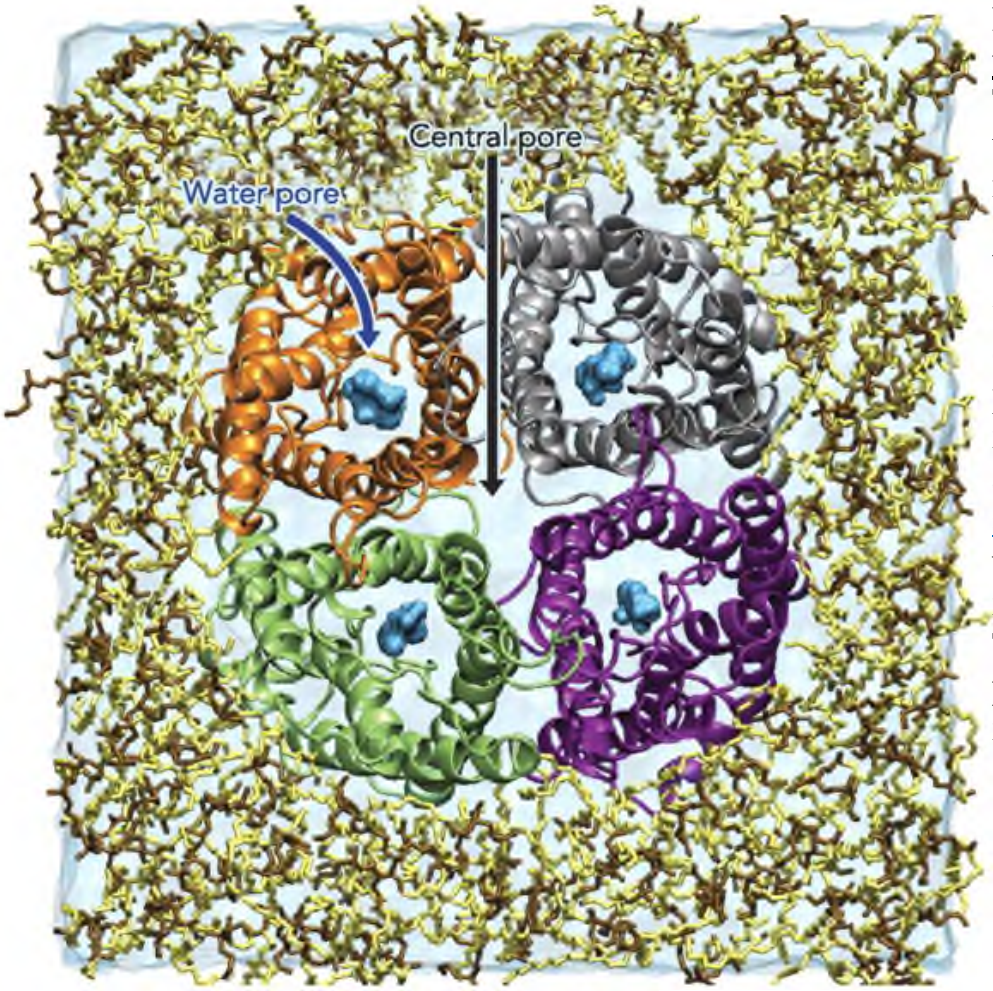

FIGURE 2. Membrane protein simulation system. Top **(A)** and side view **(B)** of the simulation system of a mammalian **AQP**1 **tetramer** embedded in a pure POPE **bilayer**. In the side view, the front **monomer** is removed for clarity. **Water** molecules permeating **water pore**s within individual **AQP**1 **monomer**s are represented by a **blue** space-filling representation, whereas bulk **water** is shown in a **light blue** transparent box. The locations of the **water pore**s and the **central pore** are indicated by arrows.

(A)

(B)Water channels H_2O and **O_2,NO**,**CO** Physiology 2010 vol. 25 no. 3 142-154 **1J4N**

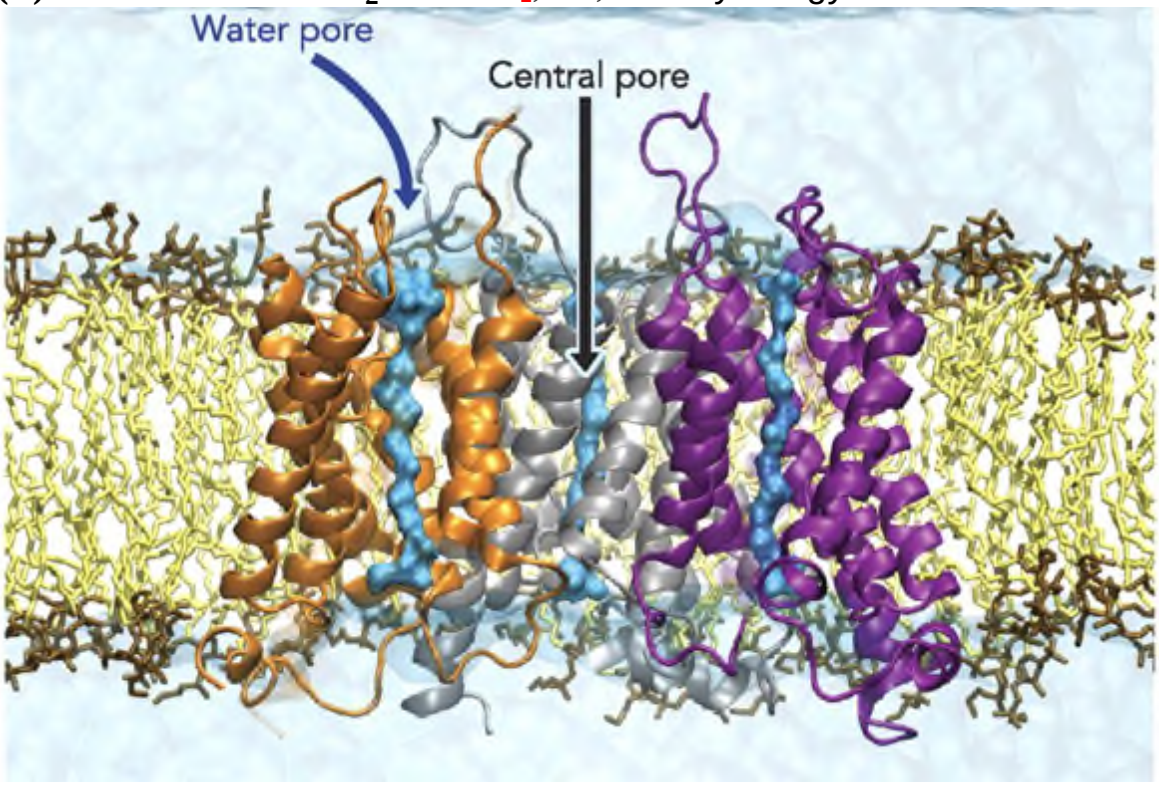

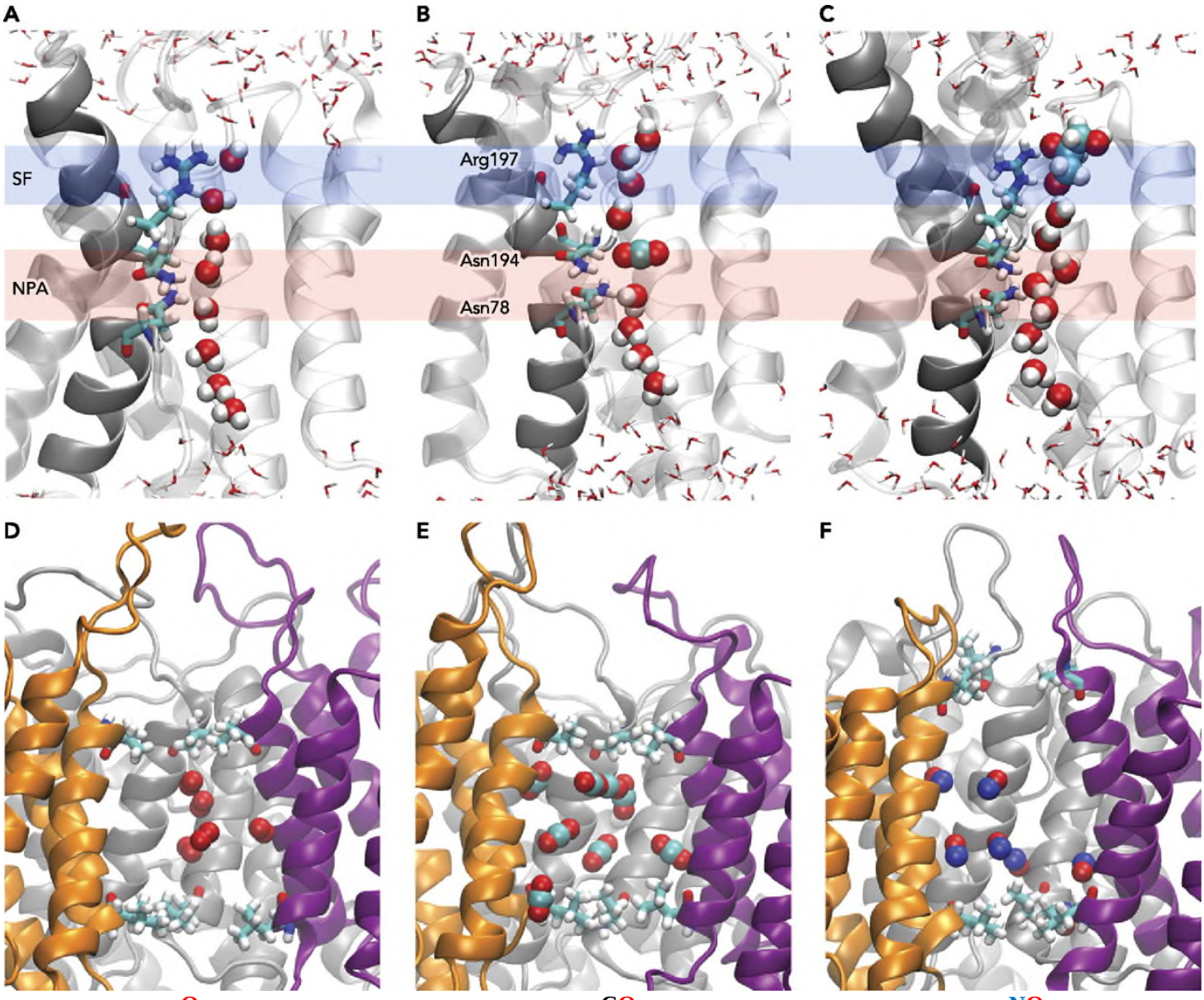

FIGURE 3. Conduction pathways for small molecules in AQPs. *A–C* **conduction** of **water**, **O_2**, **NO**, **CO**, **CO_2 (A)**, **CO_2 (B)**, and **glycerol (C)** by the **water pore**s of **AQP**s (64, 113). *D–F*: spontaneous entrance and accumulation of **O_2 (D)**, **CO_2** (*E*), and **NO** (*F*) in the **central pore** captured during equilibrium MD simulations (113, 117). The bi**polar** orientation of **water** can be seen in *A*, where **water** molecules in both halves of the **channel** point their **oxygen** toward the **center** of the **pore**. **two half-membrane** spanning **helices** (**dark gray**) and the **asparagine residue**s (**Asn**) from the **NPA motif**s, along with the conserved **arginine** (**Arg**) in the **selectivity filter (SF)** are shown in *A–C*. The outermost **hydrophobic residue**s defining the **narrow**est regions in the **central pore** are explicitly shown in *D–F*.

Energetics of Substrate Permeation Through the Water Pores Given adequate sampling, the **energetic**s associated with the molecular phenomenon at hand can be readily calculated from MD simulations. Since **water permeation** through the **water pore**s of **AQP**s happens on a **nanosecond** time scale, all reported equilibrium MD simulations (21, 45, 63, 84, 101, 102, 105, 113, 117, 123) have been able to collect ample sampling on the dynamics of **water** inside the **water pore**s. The relatively fast **translocation** of **water** in the **water pore**s has resulted in adequate sampling of all points along the **pore** axis in all reported equilibrium MD simulations (21, 45, 63, 84, 101, 102, 105, 113, 117, 123) from which a **free energy** profile for **water permeation** can be reconstructed based on the probability distribution of **water** along the **pore**. Calculations based on this method have shown that **water permeation** through the **water pore**s of **AQP**s requires crossing **barrier**s of ~3 kcal/mol (see Table 1) (55, 117).

Free energy barriers against permeation of water and small gas molecules in AQPs and lipid bilayers. The values are collected from MD simulations performed on human **AQP**1 (55), bovine**AQP**1 (113), rat **AQP**4 (117), E. coli GlpF (55), and **two** model **lipid bilayer**s, POPE (55, 117) and POPC (55).

Table 1.

	Water Pore			Central Pore			Lipid Bilayer	
Molecule	h**AQP**1	b**AQP**1	**AQP**4	GlpF	b**AQP**1	**AQP**4	POPE	POPC
O_2	6.5*	5.7‡	4.9	3.0*	3.6‡	2.9	0.4	1.0†
CO_2	5.3*			3.2*	3.6‡		1.0†	0.4†
NO			5.8			2.9	0.3	
NH_3	4.3*			3.0*			4.5†	3.6†
H_2O	3.4		3.0	3.2			7.4†	6.4†

All values are in kcal/mol.

* Statistical error of ≤0.6 kcal/mol (55).

† Statistical error of ≤0.5 kcal/mol (55).

‡ Statistical errors for these results are obtained as described in Ref. 15. The upper bound error is ≤0.25 kcal/mol, and the lower bound errors are less than/equal to −1.7 kcal/mol and ≤0.6 kcal/mol for the **water pore** and the **central pore**, respectively (113).

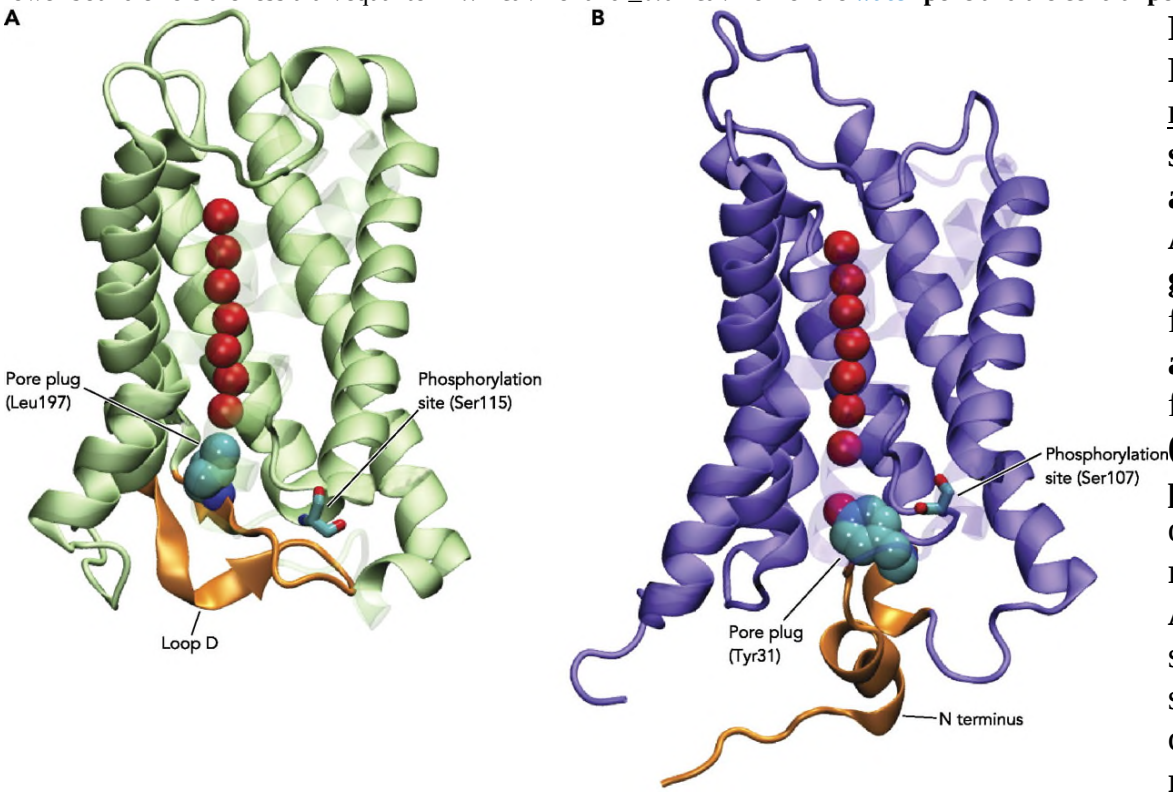

FIGURE 4. Proposed gating mechanisms for a spinach aquaporin and for yeast AQY1 Proposed **gating** mechanisms for a spinach **aquaporin (A)** and for yeast **AQY**1 **(B)**. On **phosphorylation** of conserved **serine residue**s, the **two AQP channel**s switch to an open state through the coupling of a **plug residue** (**Leu197** in SoPIP2;1 and **Tyr31** in **AQY**1) and a **cytoplasm**ic region of the protein (***loop D*** in SoPIP2;1 and the **N-terminus** in **AQY**1; shown in **orange**). The **N-terminus** of **AQY**1 is also suggested to act as a **sensor** to the **membrane** tension (32).

In addition to circumstantial evidence (i.e., specific subcellular localization of **Aqp1**ab in the oocyte correlating with the **hydration** process), the physiological role of **Aqp1**ab is supported by the observation that the swelling of oocytes undergoing meiosis resumption is completely or partially blocked by **aquaporin** inhibitors, such as mercury and tetraethylammonium (Fabra et al. 2005, 2006; Kagawa et al. 2009). However, it is known that these compounds can also affect K^+ **channels** and other ion transport proteins (Armstrong 1990; Jacoby et al. 1999), which may play a role for inorganic osmolyte accumulation in the oocyte (Cerdà et al. 2007; Kristoffersen and Finn 2008). Therefore, direct evidence for the role of **Aqp1**ab during fish oocyte **hydration** is still lacking. In addition, although the majority of teleost **aquaporin**s appear to have arisen as a consequence of whole-genome duplication (WGD) (Tingaud-Sequeira et al. 2010), the ***Aqp1aa*** and ***-1ab*** genes were suggested to be the result of tandem duplication (Tingaud-Sequeira et al. 2008). To address these issues, we selected the Atlantic halibut (*Hippoglossus hippoglossus*) as an experimental model because it is a marine acanthomorph teleost that reproduces at low temperature and spawns one of the largest pelagic eggs known. We isolated two novel **aquaporin**-1 transcripts and examined the functional role of **Aqp1**ab during meiosis resumption using ex vivo and in vivo approaches. To determine the duplication history of the teleost ***Aqp1aa*** and ***-1ab*** genes, we reexamined the molecular phylogeny of the transcripts and deduced proteins in relation to 26 vertebrate orders. These data revealed that tetrapod ***AQP1*** and teleost ***Aqp1aa*** orthologs have experienced purifying selection within each clade, whereas the teleost ***Aqp1ab*** orthologs displayed a paralogous subclustering topology. To determine whether a given subcluster could represent the product of WGD, an extended synteny analysis was performed for selected tetrapod and teleost genomes. Mol Biol Evol *(2011) 28 (11): 3151-3169.* Volume 28,, Issue 11 Pp. 3151-3169. **1J4N**

Supplementary Figure S1. Structural features of vertebrate aquaporin-1 orthologs.

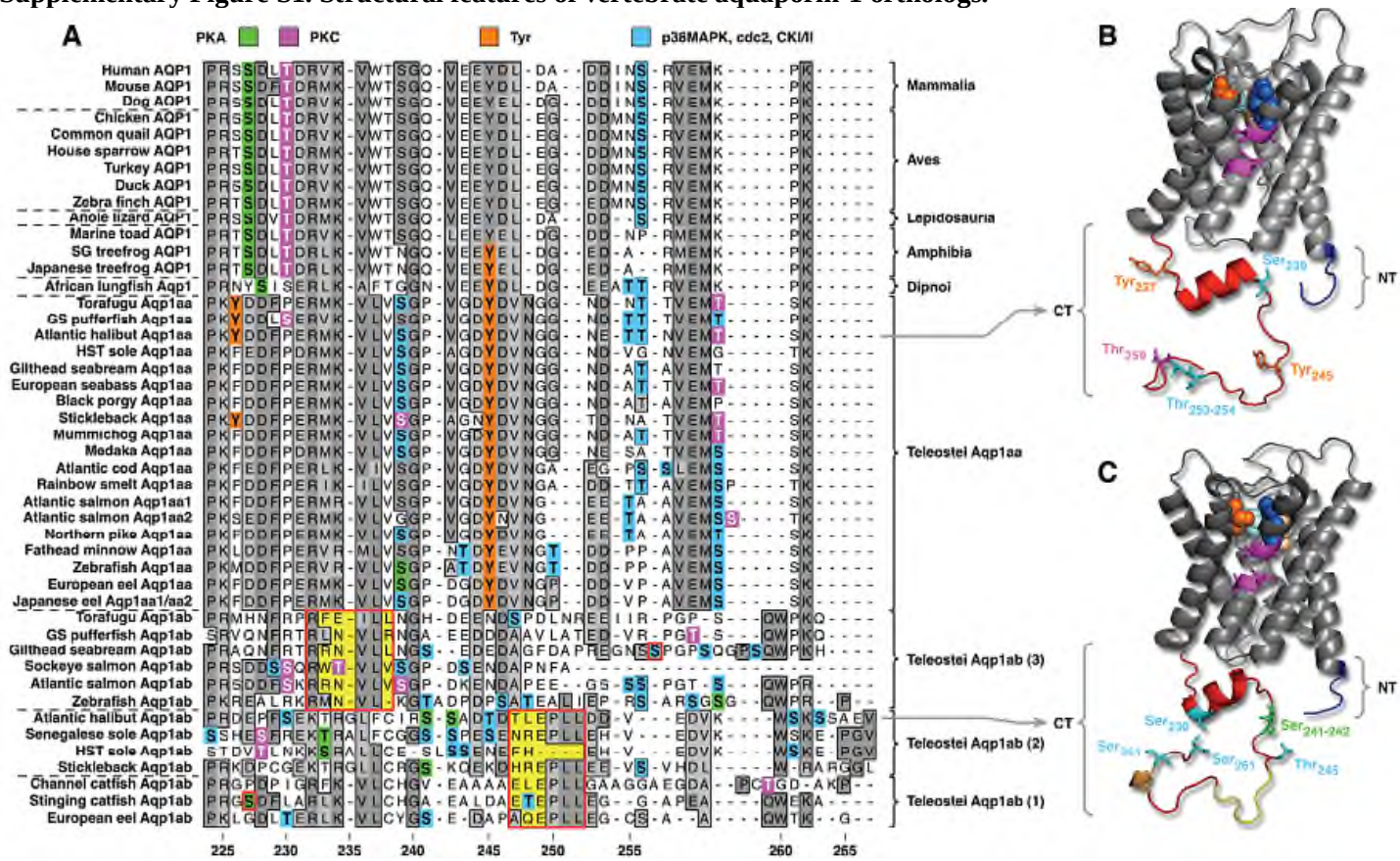

(A) Alignment of **C-terminal** domains illustrating known and putative **phosphorylation** sites. In gilthead seabream and stinging catfish **Aqp1**ab **phosphorylation** of **Ser254** and **Ser227**, respectively outlined with **red boxes**, have been shown to play opposite roles in **intracellular traffick**ing (Tingaud-Sequeira et al., 2008; Chaube et al., 2011). Highly conserved residues are boxed and shaded in **dark grey**. Residues with similar chemical properties are shaded in light grey. Residue numbers below the alignment are annotated for Hh**Aqp1**ab. (**B** and **C**) Three-dimensional models of Hh**Aqp1**aa **(B)** and Hh**Aqp1**ab **(C)** illustrating the conserved **transmem-brane helices** (1, 2, 4, 5, 6 and 8) and the **two intramembranous hemi-helices** (**3** and **7**) that bear the conserved **Asn-Pro-Ala** (**NPA**) **motifs.** Residues associated with the **ar/R constriction** are rendered as spacefill: **Phe50** (**pale blue**), **His172/171** (wheat), **Arg187/186** (**Blue**), and the putative **mercury-sensitive** residues **Cys181/180** (**orange**). **C-termini** are rendered as cartoons in **red** with stick renders of the predicted **phosphorylation** sites highlighted in **(A). water, O_2, NO, CO, CO_2**